environmental microbiology

Environmental Microbiology (2018) **20**(11), 3980–3991 doi:10.1111/1462-2920.14426

Pseudomonas syringae evades phagocytosis by animal cells via type III effector-mediated regulation of actin filament plasticity

Sung-Jin Yoon,[1†] Young-Jun Park,[1,2†] Jun-Seob Kim,[3] Soohyun Lee,[3] Sang-Hyun Lee,[4] Song Choi,[1] Jeong-Ki Min,[4] Inpyo Choi[2,5] and Choong-Min Ryu[3,6*]

[1]*Metabolic Regulation Research Center, KRIBB, Yuseong-gu, Daejeon 34141, South Korea.*

[2]*Department of Functional Genomics, University of Science and Technology (UST), Yuseong-gu, Daejeon, 34141, Republic of Korea.*

[3]*Infectious Disease Research Center, KRIBB, Yuseong-gu, Daejeon 34141, South Korea.*

[4]*Biotherapeutics Translational Research Center, KRIBB, Yuseong-gu, Daejeon 34141, South Korea.*

[5]*Immunotherapy Convergence Research Center, KRIBB, Yuseong-gu, Daejeon, 34141, South Korea.*

[6]*Biosystems and Bioengineering Program, University of Science and Technology (UST), Yuseong-gu, Daejeon, 34141, Republic of Korea.*

Summary

Certain animal and plant pathogenic bacteria have developed virulence factors including effector proteins that enable them to overcome host immunity. A plant pathogen, *Pseudomonas syringae* pv. *tomato* (*Pto*) secretes a large repertoire of effectors via a type III secretory apparatus, thereby suppressing plant immunity. Here, we show that *Pto* causes sepsis in mice. Surprisingly, the effector HopQ1 disrupted animal phagocytosis by inhibiting actin rearrangement via direct interaction with the LIM domain of the animal target protein LIM kinase, a key regulator of actin polymerization. The results provide novel insight into animal host–plant pathogen interactions. In addition, the current study firstly demonstrates that certain plant pathogenic bacteria such as *Pto* evade phagocytosis by animal cells due to cross-kingdom suppression of host immunity.

Received 10 July, 2018; revised 18 September, 2018; accepted 18 September, 2018. *For correspondence. E-mail cmryu@kribb.re.kr. Tel. +82-42-879-8229; Fax +82-42-860-4488. †These authors contributed equally to this work.

Introduction

Bacterial infection normally shows a tightly regulated host specificity in which the ability to colonize is dependent on species-specific molecular interactions (e.g., porin proteins, type IV pili and proteases) that determine the host range of the pathogen (Pan *et al*., 2014). Despite this, some bacteria show cross-kingdom pathogenicity (van Baarlen *et al*., 2007; Kirzinger *et al*., 2011; Whittaker *et al*., 2016). A previous study highlights the ability of specialized plant-associated bacteria to cause human and animal diseases or *vice versa* (Kirzinger *et al*., 2011). Six genera (*Salmonella*, *Serratia*, *Enterobacter*, *Enterococcus*, *Pantoea* and *Burkholderia*) cause symptoms in both plants and mammals, either directly or after transmission by vectors such as insects (Kirzinger *et al*., 2011); however, the mechanisms by which these plant pathogens evade the innate immune system in animals remain unclear. To infect a host belonging to a different kingdom, a pathogen must first evade or overcome the immune system long enough to establish a colony. Thus, the innate immune (nonantigen-specific) system in the host organism plays an essential role in host defence and is the first hurdle that a pathogenic bacterium must overcome (Medzhitov and Janeway, 2000).

Phagocytes such as macrophages, neutrophils and dendritic cells act as the cellular effector branch of the mammalian innate immune system. Phagocytosis is triggered by recognition of pathogens by cell surface receptors; the engulfed pathogens are then digested within phagolysosomes (Underhill and Goodridge, 2012; Settembre *et al*., 2013). Clearance of infected pathogens is a well-orchestrated process that involves various steps, including recognition, internalization, phagosome formation/digestion and elimination of debris (Settembre *et al*., 2013; Gordon, 2016). Phagocytosis, especially internalization, requires actin (de)polymerization before bacteria are engulfed. This process includes formation and closing of a phagocytic cup, which occurs via membrane

protrusion and retraction (Swanson, 2008). (De)phosphorylation of cofilin1 (Mizuno, 2013), a ubiquitous and abundant actin-binding factor, plays an important role in actin dynamics by regulating polymerization/depolymerization (Galkin *et al*., 2011). Innate immune responses, and thus, host defence, depend on regulation of actin by cofilin1 (Mostowy and Shenoy, 2015). LIM domain kinase 1 (LIMK1) is a serine/threonine protein kinase that also plays an essential role in regulating actin filament dynamics (Mizuno, 2013). LIMK1 regulates (de) phosphorylation of cofilin1; therefore, expression of LIMK1 and internalization of bacteria by phagocytes are linked directly (Bierne *et al*., 2001). Some animal pathogenic bacteria regulate actin dynamics in phagocytes either directly or indirectly; this is one mechanism by which bacteria evade the mammalian immune system (Stevens *et al*., 2006; Hybiske and Stephens, 2008).

Similar to cofilin-mediated actin rearrangement in animal cells, the actin (de)polymerization factor-based cytoskeleton network plays a critical role in plant immunity (Li and Staiger, 2018). In plants, actin-associated proteins facilitate growth, breakdown and rearrangement of the cytoskeleton, which performs specific immune-related functions (Day *et al*., 2011; Porter and Day, 2015). The growth of plant pathogenic microbes within the intercellular space is suppressed by defence components such as pathogenesis-related (PR) proteins and phytoalexins, which are secreted via the actin-based cytoskeleton network (Guo *et al*., 2016). Various plant pathogens harbour virulence factors that target the host cytoskeleton specifically, including actin dynamics (Porter and Day, 2015). Disrupting this network results in impaired secretion of PR proteins and phytoalexins and, consequently, weakens the plant's defence against infection. Thus, disrupting host immunity by regulating actin dynamics via specific bacterial effectors is a common virulence mechanism used by both plant and human pathogens.

Due to difficulties inherent in studying pathogens in different kingdom hosts, few studies have examined the activity of effectors produced by plant pathogenic species in animal cells; therefore, there is no evidence that effectors secreted by plant pathogenic bacteria also target the actin filament system in animal cells. Initially, we asked whether the actin filament network plays an important role in both the animal and plant innate immune systems, and whether pathogens regulate actin filament dynamics to facilitate immune system disruption; if so, plant pathogens might regulate phagocytosis in animal hosts. Here, we demonstrate that inoculating mice with the plant pathogenic bacterium *Pseudomonas syringae* pv. *tomato* (*Pto*), a well-defined plant pathogen used to study interactions between hosts plants such as tomato and *Arabidopsis* and bacteria (Xin and He, 2013), causes sepsis. In addition, we found that the type III effector HopQ1, which is secreted by *Pto*, interacts with the mammalian target protein LIMK1 to inhibit phagocytosis, thereby suppressing the mammalian immune response. These results indicate that HopQ1 manipulates actin filament dynamics by regulating the activity of cofilin1 via phosphorylation of LIMK1. These data provide the first evidence of a molecular mechanism by which plant pathogenic bacteria disrupt immune responses in order to establishing full virulence in animal cells.

Results

Pseudomonas syringae *suppresses an early step during macrophage-mediated phagocytosis*

Because of the striking similarities between the innate immune systems of animals and plants (Nurnberger *et al*., 2004; Ausubel, 2005; Selosse *et al*., 2014), we wanted to determine whether a plant pathogen could attenuate the immune response of an animal host cell. To this end, we used flow cytometry and confocal microscopy to examine infection of murine peritoneal macrophages by two green fluorescent protein (GFP)-tagged plant pathogens [*P. syringae* pv. *tomato* (*Pto*-GFP) and *P. syringae* pv. *tabaci* (*Pta*-GFP)] since they are well-studied plant pathogens; no reports of their ability to infect animal hosts have been reported. Interestingly, after a 2 h incubation the number of GFP-positive macrophages harbouring *Pto*-GFP was significantly lower than that harbouring *Pta*-GFP or *E. coli*-GFP (used as a control) (Fig. 1A). Confocal microscopy images showed clearly that macrophages (blue) were less able to engulf *Pto*-GFP (green) than the other bacterial strains (Fig. 1B). Since flow cytometry signals and plain images from confocal microscopy provide no information about the subcellular localization of plant pathogens, we reconstructed Z-stack images (*X*-*Z* plane) of the *Pta* or *Pto*/macrophage complexes. These images suggest that, unlike *Pta*-GFP, *Pto*-GFP was attached to the surface of the macrophages rather than being internalized (Fig. 1C, white arrows). In addition, a gentamycin protection assay (Laroux *et al*., 2005) revealed that macrophages internalized *Pto* to a lesser extent than *Pta* or *E. coli.* The number of internalized bacterial cells [expressed in terms of the number of colony-forming units (CFUs)] was determined after treatment with gentamycin to remove surface-attached bacteria (Fig. 1D).

Since phagocytosis involves not only internalization of bacteria but also phagosome maturation (Underhill and Goodridge, 2012; Gordon, 2016), we performed additional assays to confirm phagosome maturation in macrophages by measuring elimination of internalized bacteria and expression of phagosomal markers. The reduction of bacterial GFP signal 'in macrophages' was quantified by flow cytometry during incubation since it represents the number of internalized bacteria; reduction of GFP signal indicates clearance of bacteria in the macrophage. Although the number of internalized *Pto* cells was lower than the

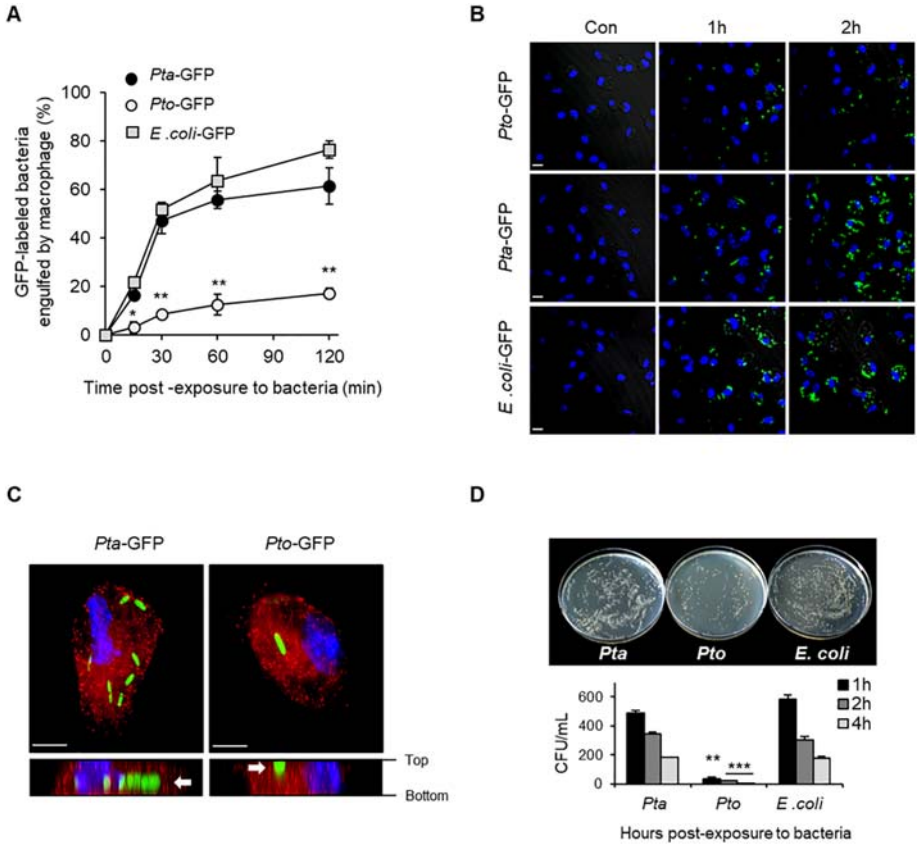

Fig. 1. A plant pathogen, *Pseudomonas syringae* pv. Tomato, avoids phagocytic engulfment by mouse peritoneal macrophages. A. Peritoneal macrophages from C57BL/6 mice were incubated with GFP-expressing *Pta*, *Pto* or *E. coli* [multiplicity of infection (MOI), 20:1] for the indicated times. Macrophages were analysed by flow cytometry. Data are expressed as the mean ± SD, calculated from three different wells per time point (**P* < 0.05 and ***P* < 0.01, compared with *Pta*). B. Phagocytosis by mouse peritoneal macrophages was examined by immunofluorescence analysis. GFP-expressing *Pto*, *Pta* or *E. coli* were fixed and analysed under a confocal laser microscope (LSM510; Carl Zeiss). Scale bars, 20 μm. C. Peritoneal macrophages were infected for 30 min with GFP-expressing *Pto* or *Pta* (MOI, 20:1) and then washed and fixed. Cells were then stained with a primary antibody specific for Rab5, followed by an Alexa Fluor 555-conjugated secondary antibody. All images were analysed by confocal microscopy. D. Internalized bacteria were detected in a gentamicin protection assay. Bacterial replication was expressed in terms of colony-forming units (CFUs). Data are expressed as the mean ± SD, calculated from three different plates per time point (***P* < 0.01 and ****P* < 0.001, compared with *Pta*).

number of internalized *Pta* and *E. coli* cells, all internalized bacteria belonging to each of the three species were eliminated after incubation with macrophages, suggesting cell lysis within the phagosome (Supporting Information Fig. S1A). There was no difference in expression of early (Eea1 and Rab5) or late (Rab7 and Lamp1) phagosomal markers, indicating equivalent phagosome maturation in response to infection with each of the three species (Supporting Information Fig. S1B) (Kinchen and Ravichandran, 2008; Flannagan *et al*., 2009). These results indicate that, during infection by *Pto*, phagocytosis by macrophages was inhibited at an early stage (internalization) rather than at a late stage (phagosome maturation).

Bacterial type III secretion plays a pivotal role in inhibiting phagocytosis both in vitro *and* in vivo

Many pathogenic Gram-negative bacteria, including *Pto*, use type III secretion systems (T3SSs) to secrete effector proteins directly into the host cytosol. In most cases, these effectors disrupt or inhibit host defence mechanisms (Coburn *et al*., 2007). Since the plant pathogen *Pto* inhibited the early stage of phagocytosis by macrophages, we hypothesized that T3SS-derived effectors play a pivotal role in suppressing phagocytosis. To verify this, we used *Pto* Δ*hrpL*, which lacks a T3SS (i.e., a T3SS-null mutant) (Sreedharan *et al*., 2006). As expected, flow cytometry analysis (Fig. 2A), a gentamycin protection assay (Fig. 2B), and confocal microscopy analysis (Fig. 2C) of *Pto* Δ*hrpL* revealed recovery of phagocytosis. This observation was reproduced in a macrophage cell line, RAW 264.7 (Supporting Information Fig. S2A). Compared with wild-type (WT) *Pto*, no significant changes in expression of phagosome markers were observed after infection with Δ*hrpL* (Supporting Information Fig. S2B). Hence, secretion of effectors via the T3SS controls phagocytosis at an early stage: internalization of bacteria.

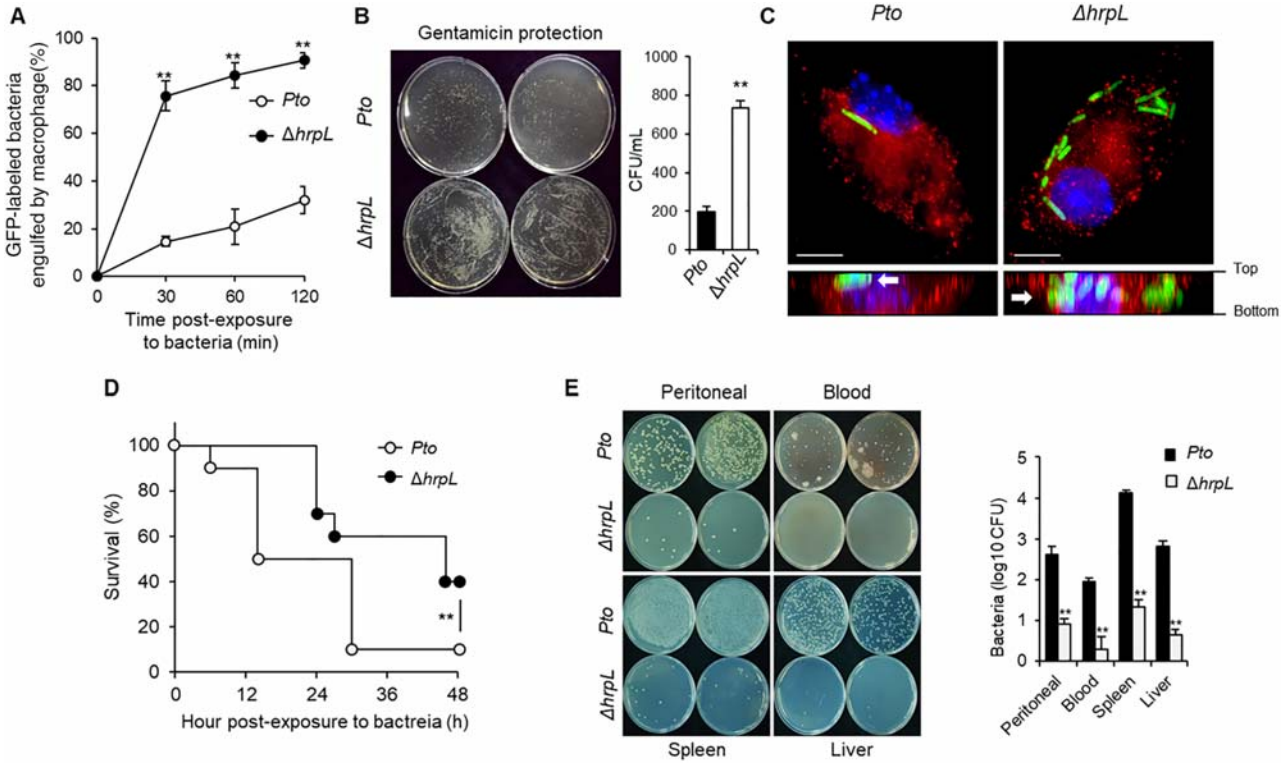

Fig. 2. Deletion of the type III secretion system restores engulfment of mouse macrophages. A. Peritoneal macrophages were infected with GFP-expressing *Pto* or Δ*hrpL* (MOI, 20:1) for the indicated periods, washed, scraped from the plate and then fixed. Retained bacteria were analysed by flow cytometry. Data are expressed as the mean ± SD, calculated from three different wells per time point (**$P < 0.01$). B. Mouse peritoneal macrophages were infected with *Pto* or Δ*hrpL*, and the bacterial population was measured via a gentamicin protection assay. Data are expressed as the mean ± SD, calculated from three different plates per time point (**$P < 0.01$). C. Peritoneal macrophages were infected for 30 min with GFP-expressing *Pto* or Δ*hrpL* (MOI, 20:1) and then washed, fixed and stained with a primary antibody specific for Rab5, followed by an Alexa Fluor 555-conjugated secondary antibody. All images were acquired by confocal microscopy. D. *Pto* or Δ*hrpL* [10^8 colony-forming units (CFUs) of live bacteria] was injected intraperitoneally (i.p.) into C57BL/6 mice ($n = 10$). Survival was assessed every 2 h (**$P < 0.01$, compared with *Pto*). (E) *Pto* or Δ*hrpL* was injected i.p. into C57BL/6 mice ($n = 5$). After 24 h, PBS lavage samples from the peritoneal cavity, blood, spleen and liver were plated on agar and incubated for 24 h. Bacterial populations were measured by counting the number of CFUs. Data are expressed as the mean ± SD, calculated from three different plates per time point (**$P < 0.01$, compared with *Pto*).

Since the plant pathogen *Pto* was able to escape phagocytosis in murine macrophages, we examined the susceptibility of mice to infection by *Pto* to determine whether a plant pathogen could cause sepsis in a host from a different kingdom. Intraperitoneal injection of *Pto* WT and Δ*hrpL* caused death within 50 h. Interestingly, more of the mice injected with *Pto* Δ*hrpL* survived (about 50% at 50 h), while injection of *Pto* WT resulted in a 20% survival rate at the same time point (Fig. 2D). At 24 h post-injection, the numbers of bacterial cells in the peritoneal cavity, blood, spleen and liver of mice challenged with *Pto* Δ*hrpL* were markedly lower than those in organs from WT mice (Fig. 2E). Likewise, terminal deoxynucleotidyl transferase dUTP nick-end labeling (TUNEL) assays and haematoxylin and eosin (H&E) staining revealed that the number of apoptotic cells in the liver, spleen and lung following infection with *Pto* Δ*hrpL* was significantly lower than that following infection with wild type *Pto* (Supporting Information Fig. S3A). Aspartate transaminase (AST) and alanine transaminase (ALT) levels in blood samples suggested a lower level of hepatic damage in *Pto* Δ*hrpL*-infected mice (Supporting Information Fig. S3B). Taken together, these results suggest that effectors secreted via the T3SS successfully inhibit phagocytosis *in vivo.*

Type III effectors inhibit actin-mediated early phagosome formation

In the animal immune system, macrophages act as gatekeepers that fight bacterial infection; however, bacteria have evolved various mechanisms to escape capture by these cells (Hybiske and Stephens, 2008; Sarantis and Grinstein, 2012). Some animal pathogens produce actin-related proteins to regulate actin polymerization (Frischknecht *et al*., 1999; Gouin *et al*., 1999), which is important for phagocytosis (Coppolino *et al*., 2001; Blanchoin *et al*., 2014). We showed that T3SS-derived

effectors inhibit internalization of *Pto* by suppressing phagocytosis by macrophages; therefore, we investigated actin-related phagosome formation further. F-actin accumulated in the cell membranes of peritoneal macrophages during infection by *Pto*; however, accumulation of F-actin was observed only around engulfed bacteria in the phagosome (total F-actin) after infection with *Pto* Δ*hrpL* (Supporting Information Fig. S4). To investigate this in greater detail, we examined remodelling of RAW 264.7 macrophages through changes in the actin cytoskeleton during bacterial infection. First, measurement of F-actin accumulation only in the phagosome (phagosomal F-actin) indicated that phagosome formation was restored in the absence of type III effector (Δ*hrpL*) secretion (Fig. 3A). Second, time-lapse observation of RAW 264.7 macrophages during bacterial infection revealed that both the number and frequency of phagocytic cups were significantly higher in cells infected with Δ*hrpL* (Fig. 3B and Supporting Information Fig. S5). Additionally, *Pto* inhibited protrusion and retraction to a greater extent than the Δ*hrpL* mutant (Fig. 3C). Since the protrusion and retraction steps of cup formation are the critical steps in F-actin-mediated early phagosome formation (Swanson, 2008), we examined phosphorylation of two key factors during actin regulation: LIMK1 and cofilin1, which regulate transient actin polymerization and depolymerization (Bravo-Cordero *et al*., 2013). Interestingly, infection with *Pto* induced marked phosphorylation of LIMK1 and cofilin1, whereas infection with *Pto* Δ*hrpL* did not (Fig. 3D). LIMKs are serine/threonine kinases that are activated by other kinases through phosphorylation. Phosphorylated LIMK1 causes phosphorylation and subsequent inactivation of cofilin1, which then regulates actin polymerization/depolymerization (Bravo-Cordero *et al*., 2013). These events inhibit phagocytic cup closure (Bierne *et al*., 2001). Overall, these findings strongly suggest that inhibition of phagocytosis by T3SS-related effectors secreted by *Pto* occurs via deregulation of actin polymerization/depolymerization, which is induced by phosphorylation of LIMK1/cofilin1.

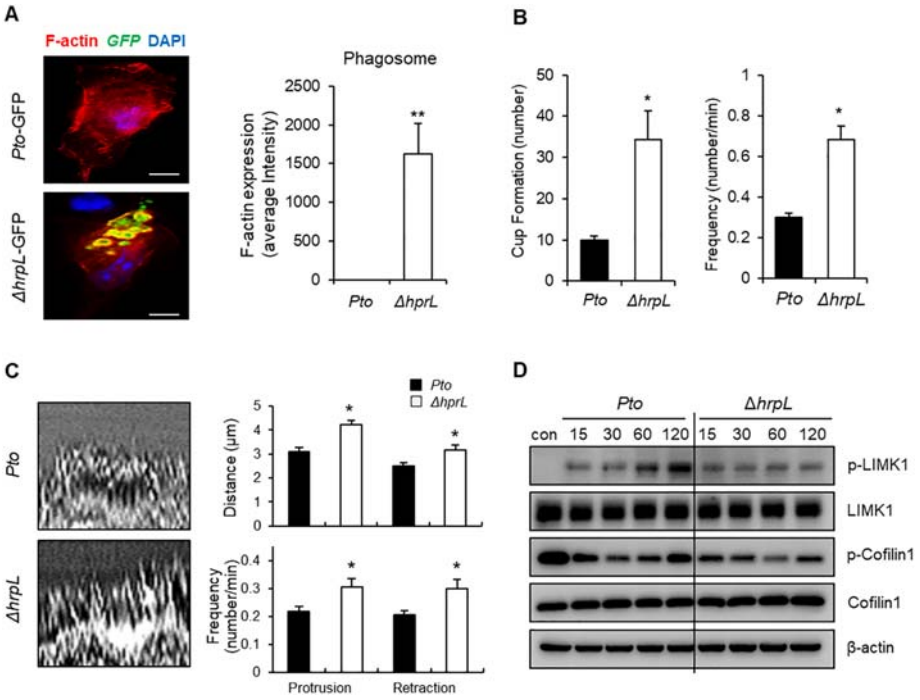

Fig. 3. T3SS-mediated effectors secreted by the plant pathogen *Pto* inhibit actin-mediated early phagosome formation. A. RAW 264.7 cells were infected with GFP-labelled *Pto* or ▽*hrpL*. After 30 min, cells were fixed and stained with phalloidin to examine F-actin. The intensity of F-actin expression was measured using Metamorph software (n = 25). Scale bar, 5 μm (**P < 0.01, compared with *Pto*). B. Temporal analysis of phagocytic cup formation by macrophages. Images were acquired at 15 s intervals for 30 min after infection of cells with *Pto*-GFP or Δ*hrpL*-GFP. For each group, phagocytic cup formation by at least 10 individual cells was monitored for 30 min and the frequency was analysed using Metamorph software (*P < 0.05, compared with *Pto*). C. Deletion of *hrpL* led to a notable increase in membrane ruffle formation. Lamella dynamics were analysed using kymographs. For each group, membrane ruffles in at least 10 individual cells were monitored over a 15 min period by capturing digital images every 6 s. Subsequently, three areas of interest were marked on each image using lines that crossed the cell lamella. Kymographs were then assembled using Metamorph software, and ruffle formation was quantified. Data are from one experiment representative of five. D. Mouse macrophages were infected with *Pto* or Δ*hrpL* (MOI, 20:1) at the indicated times, and expression of LIMK1, p-LIMK1, p-cofilin1, cofilin1 and β-actin was examined by immunoblot analysis.

The bacterial type III effector HopQ1 is central to inhibition of phagocytosis

Pto harbours at least 28 effectors that are fully active and expressed at levels detectable in a type III effector translocation assay in *Arabidopsis* and tomato plants (Cunnac *et al*., 2009). To identify the key effector protein(s), we examined phagocytosis of the *Pseudomonas fluorescens* EtHAn (Effector-to-Host Analyzer) strain that is nonpathogenic but was engineered to express the structural T3SS, and that of variants expressing 16 individual T3SS effectors. A gentamycin protection assay revealed that overexpression of HopQ1 clearly inhibited internalization of *P. fluorescens* EtHAn by macrophages (Fig. 4A). Additionally, *P. fluorescens* EtHAn expressing HopQ1 induced phosphorylation of LIMK1 and cofilin1 in macrophages (Fig. 4B). Furthermore, and similar to infection by wild type *Pto*, overexpression of HopQ1 by macrophages increased phosphorylation of both LIMK1 and cofilin1 (Fig. 4C). To confirm translocation of HopQ1 from the bacterial cytosol to that of the animal cell, we transfected *Pto* WT, two T3SS-deficient mutants (Δ*hrcC* and Δ*hrpL*) and Δ28E (lacking 28 effectors) with a plasmid expressing a *hopQ1-cya* fusion protein; we then performed adenylate cyclase assays. Cells infected with the two T3SS-deficient mutants showed little production of cAMP when compared with cells infected with the other three control bacterial strains (Δ28E, *Pto* WT and *P. fluorescens* EtHAn). This indicates that translocation of HopQ1 was inhibited (Supporting Information Fig. S6, two left-most columns). By contrast, cAMP levels in macrophages infected with the other three cell types in which type III secretion is intact were similar, suggesting successful translocation of HopQ1 from bacteria to the animal cell (Supporting Information Fig. S6, three right-most columns). In addition, the *Pta* strain, which did not show inhibition of phagocytosis, does not have the gene encoding HopQ1 in its genome. Therefore, HopQ1, which is translocated into macrophages via the T3SS machinery, is critical for inhibition of phagocytosis.

The effector HopQ1 interacts physically with the LIM2 domain of LIMK1

Various effector proteins secreted by *Pto* repress plant defences by targeting proteins directly involved in signalling cascades related to gene regulation. To identify the target protein of HopQ1, which induces phosphorylation of LIMK1 and cofilin1, we introduced Flag-tagged HopQ1 into a kidney cell line (293T) and performed immunoprecipitation experiments. The results showed that HopQ1 interacted directly with LIMK1, but not with cofilin1 (Fig. 5A). Since LIMK1 is located upstream of cofilin1 in the actin-regulating cascade, these data demonstrate that phosphorylated LIMK1 deactivates cofilin1 (via phosphorylation), a process induced by direct binding of LIMK to the HopQ1 effector. Co-localization of HopQ1 and LIMK1 was confirmed by confocal microscopy (Fig. 5B and Supporting Information Fig. S7).

LIMK1 contains a PDZ domain and a kinase domain (Okano *et al*., 1995). To examine how HopQ1 interacts with LIMK1, we constructed a series of LIMK1 deletion mutants lacking the LIM1, LIM2, PDZ and/or kinase domains [ΔLIM1 (lacking residues 1–76); ΔLIM1, 2 (lacking residues 1–138); ΔKinase (lacking residues 301–648); ΔPDZ, Kinase (lacking residues 148–648); and ΔLIM2, PDZ, Kinase (lacking residues 81–648)]. We

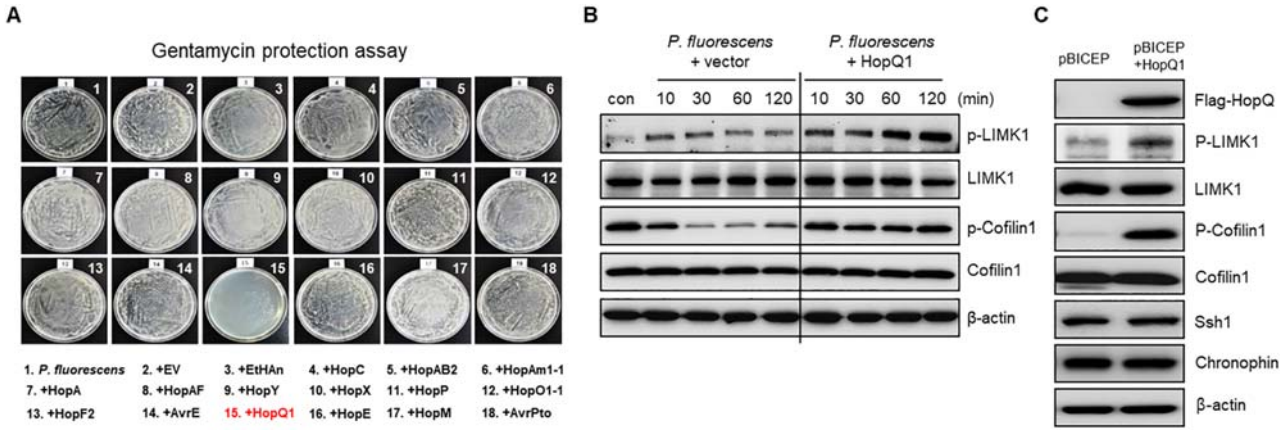

Fig. 4. The T3SS-mediated effector HopQ1 activates LIMK1 *in vitro* and increases phosphorylation of cofilin. A. Each effector protein from *P. syringae* pv. tomato DC3000 was introduced separately into *P. fluorescens* EtHAn that was engineered to express the structural T3SS. Macrophages were infected with each strain for 1 h at 37 °C, and bacterial replication was measured by determining the number of colony-forming units in a gentamicin protection assay. B. Mouse macrophages were infected with HopQ1-expressing *P. fluorescence* EtHAn (MOI, 20:1) for the indicated times, and expression of LIMK1, p-LIMK1, p-cofilin1, cofilin1 and β-actin was examined by immunoblot analysis. C. 293T cells were transfected with a control pBICEP vector or with a pBICEP vector expressing HopQ1. At 24 h post-transfection, the levels of LIMK1, p-LIMK1, p-Cofilin1, Cofilin1, Ssh1, chronophin and β-actin were determined by immunoblot analysis. Immunoblot analysis of HopQ1 expression was performed using an anti-Flag antibody.

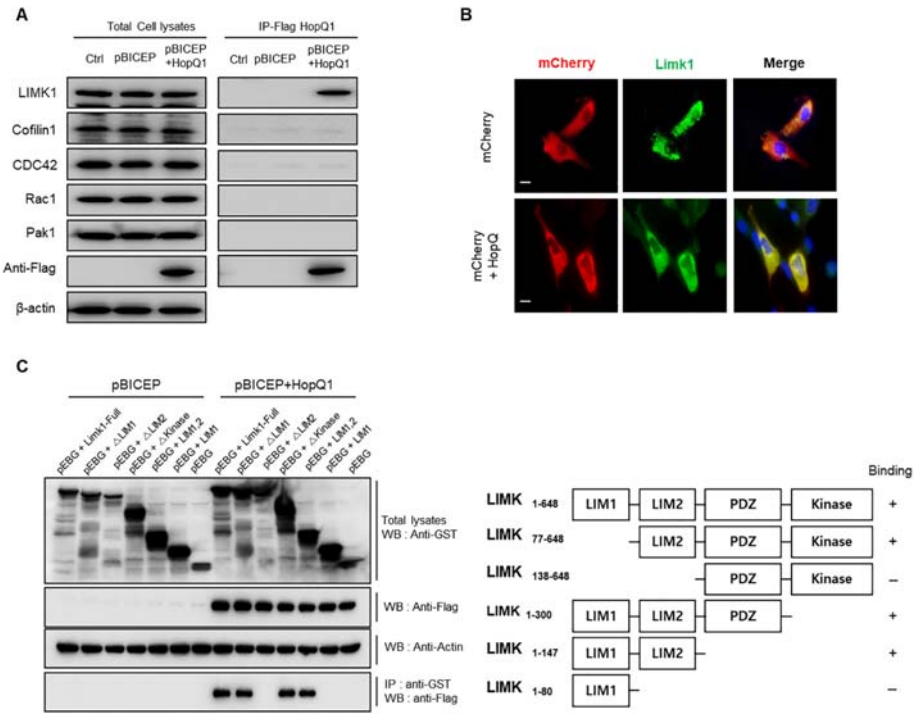

Fig. 5. The effector HopQ1 interacts directly with LIMK1 in macrophages and inhibits phagocytosis. A. 293T cells were transfected with a control pBICEP vector or with a pBICEP vector expressing HopQ1. At 24 h post-transfection, cells were harvested and cell lysates were incubated for 2 h at 4 °C with anti-DYKDDDDK (Flag)-tagged magnetic beads on a rotating apparatus. The interaction between HopQ1 and endogenous LIMK1, Cofilin1, Cdc42, Rac1 and Pak1 was examined by immunoprecipitation with an anti-Flag antibody, followed by immunoblot analysis. B. 3T3-L1 cells were transfected with either GST-LIMK1 (green) or mCherry-HopQ1 (red) and then analysed by confocal microscopy. Images show co-localization of LIMK1 and HopQ1 in 3T3-L1 cells. Scale bar, 10 μm. C. HopQ1 interacts with LIMK1 via its N-terminal LIM2 domain. HopQ1 (Flag-expressing pBICEP)- and LIMK1 (GST-expressing pEBG)-encoding vectors were co-transfected into 293T cells, and protein complexes were analysed in a GST pull-down assay, followed by western blot analysis using anti-Flag and anti-GST antibodies.

then examined their ability to interact with HopQ1 in a glutathione S-transferase (GST) pull-down assay. Bands corresponding to HopQ1 were detected only in variants containing the LIM2 domain (specifically residues 84–138; Fig. 5C). Thus, HopQ1 interacts specifically with the LIM2 domain of LIMK1, possibly leading to inhibition of macrophage-mediated phagocytosis.

Increased virulence of HopQ-transformed Enterobacter cloacae *in mice*

Next, we used *Enterobacter cloacae*, a T3SS-containing member of the normal gut flora of many mammals including humans (Krzymińska *et al*., 2009), as a surrogate host to further examine the role of HopQ1 during phagocytosis. *E. cloacae* expressing *hopQ1* gene prevented phagocytosis by peritoneal macrophages (Fig. 6A) and RAW 264.7 cells post-infection (Fig. 6B and Supporting Information Movies S1 and S2). Additionally, to confirm that HopQ1 regulates phagocytosis *in vivo*, mice were injected with *E. cloacae* expressing HopQ1, and blood, spleen and liver were examined 24 h later. Tissues from mice infected with HopQ1-expressing *E. cloacae* contained significantly more bacteria than those from mice infected with control *E. cloacae* (Fig. 6C). Based on these findings, we propose a schematic model to describe the role of HopQ1 in the immune response of macrophages (Fig. 6D). In this model, HopQ1 inhibits phagocytosis by interacting with LIMK1, the main regulator of cofilin. Phosphorylation of LIMK1 upon interaction with HopQ1 inactivates cofilin1 via phosphorylation. Thus, HopQ1 ultimately prevents phagocytosis by disrupting F-actin accumulation in macrophages.

Discussion

Phagocytosis by innate immune cells is a host defence response to infection. However, in some cases, phagocytosis can be impaired by effectors secreted by bacteria that are pathogenic to animals. Possible mechanisms include direct disruption of the phagocytic machinery or resistance to the antimicrobial factors secreted by phagocytes (Hybiske and Stephens, 2008; Kinchen and Ravichandran, 2008; Sarantis and Grinstein, 2012). For example, the human pathogen *P. aeruginosa* disrupts the actin cytoskeleton by secreting ExoT, thereby inhibiting internalization by macrophages (Garrity-Ryan *et al*., 2000). Outer membrane protein A of *E. coli* binds to complement regulatory proteins (C4b-binding protein) to provide serum-based immunity (Prasadarao *et al*., 2002). *Staphylococcus aureus* expresses complement inhibitors that break down C3 convertases to facilitate immune evasion (Rooijakkers *et al*., 2005). In particular, regulation of actin dynamics during phagocytosis to facilitate internalization of bacteria is a well-known phenomenon (Swanson, 2008); some bacteria escape host immune

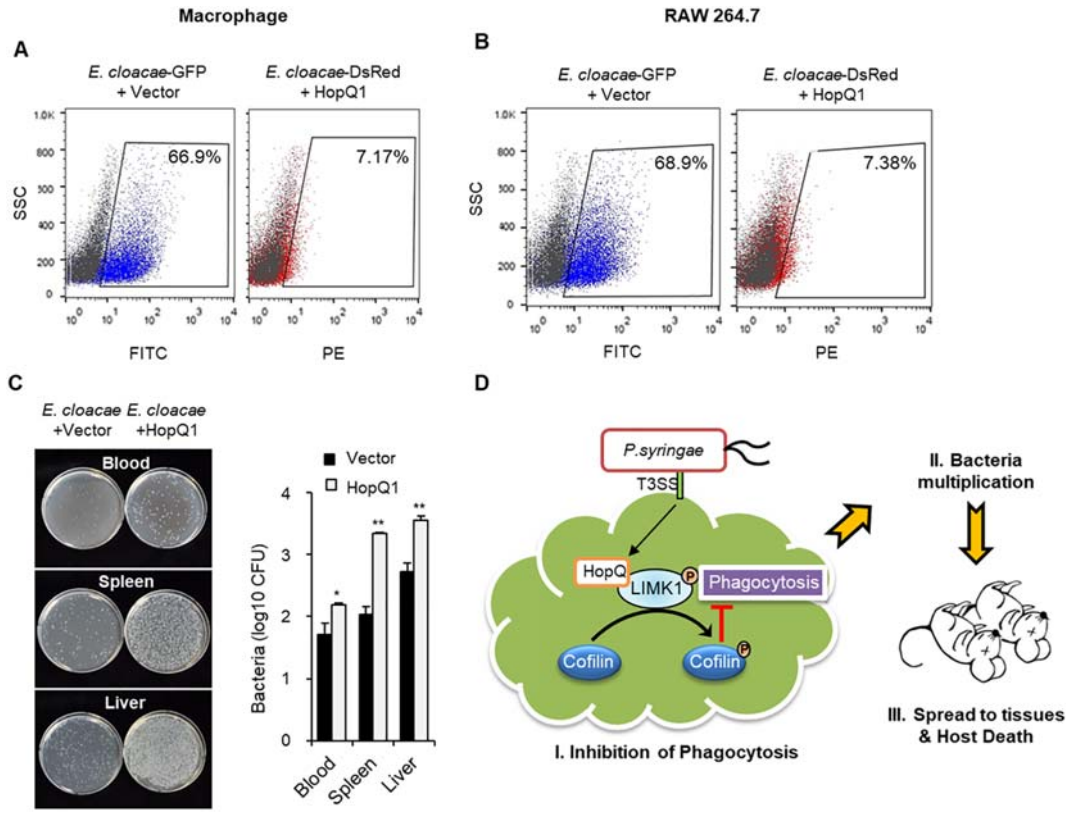

Fig. 6. Phagocytic ability of macrophages infected with GFP-expressing *E. cloacae* or with DsRed- and HopQ1-expressing *E. cloacae*. A. Mouse peritoneal macrophages were infected for 1 h with GFP-expressing *E. cloacae* or with DsRed- and HopQ-expressing *E. cloacae* and then rinsed. Bacterial elimination was examined by flow cytometry. B. RAW 264.7 macrophages were infected for 1 h with GFP-expressing *E. cloacae* or with both DsRed- and HopQ-expressing *E. cloacae* and then rinsed. Flow cytometry analysis was used to confirm bacterial elimination. C. *E. cloacae* [10^8 colony-forming units (CFUs)/mL] harbouring a HopQ1 expression plasmid (or WT *E. cloacae*) were injected intraperitoneally into C57BL/6 mice aged 10–12 weeks (n = 5). After 24 h, samples of blood, spleen and liver were plated on agar and incubated for 24 h. Bacterial replication was determined by counting the number of CFUs. Data are expressed as the mean ± SD, calculated from three different plates per time point (*P < 0.05 and **P < 0.01, compared with *E. cloacae*). D. A schematic model showing the HopQ-mediated regulatory pathways involved in *P. syringae* pv. tomato-mediated inhibition of phagocytosis. *P. syringae* pv. tomato introduces effector proteins into host cells via the type III secretory system, thereby allowing the bacterium to avoid phagocytosis. This mechanism is mediated by the bacterial effector HopQ, which binds to the LIM domain of LIMK1 to activate the protein. Activated LIMK1 phosphorylates and inhibits cofilin1.

cells by subverting actin dynamics (Frischknecht *et al*., 1999; Gouin *et al*., 1999; Stevens *et al*., 2006; Sarantis and Grinstein, 2012).

Here, we found that plant pathogen-derived type III effector, HopQ1, played a key role in regulating phosphorylation of LIMK1/cofilin1, thereby inhibiting phagocytosis during bacterial infection. We demonstrated a marked increase in phagocytic cup formation by macrophages infected with *Pto* lacking a T3SS (*Pto* Δ*hrpL*), suggesting that T3SS-related effectors secreted by *Pto* inhibit the actin assembly network. *Pto* effector-mediated regulation of the actin filament network in a plant host disrupts the plant immune system; one such example is HopG1, which targets actin within the actin filament network of plant cells (Shimono *et al*., 2016). Originally, HopQ1 was identified as a *hrp*-dependent outer protein (Hop) that is injected into plant cells by the T3SS (Alfano and Collmer, 1997). HopQ1 contains a nucleoside hydrolase-like domain, which is required for bacterial virulence (Li *et al*., 2013a). In a plant host, phosphorylated HopQ1 interacts with 14-3-3 protein, which controls functionally diverse signalling proteins (Giska *et al*., 2013; Li *et al*., 2013b). Interestingly, in animals, 14-3-3 proteins contribute to reorganization of the actin cytoskeleton by interacting with cofilin and its regulator LIMK1 (Birkenfeld *et al*., 2003). We also confirmed that HopQ1 interacts with animal 14-3-3 protein (unpublished data). The data suggest that plant HopQ1 may interact with animal 14-3-3 proteins, thereby controlling phosphorylation of LIMK1. However, the results presented herein support a physical interaction between HopQ1 and LIMK1. Similarly the interaction between HopQ1 and LIMK1, other effector proteins (e.g., HopF2 and HopAI1) interact with mitogen-activated protein kinase (MAPK) kinase (MAPKK) to disrupt the MAPK cascade (Zhang *et al*., 2007; Wang *et al*., 2010). This indicates that the Hop protein family also

regulates kinase proteins directly. Further studies are needed to confirm this.

In conclusion, to the best of our knowledge, the present study is the first to show how a plant pathogen can evade the mammalian innate immune system and cause sepsis in animals underlying cross-kingdom pathogenicity. Sepsis caused by intraperitoneal injection of a pathogenic bacterium from a different kingdom raises the following questions: how do we define the term 'Infection', and what is the Maginot line within the host defence system that determines cross-kingdom pathogenicity? Even though oral administration of *Pto* did not cause sepsis or symptoms (data not shown), plant pathogenic bacteria are potential reservoirs of infectious bacteria for humans; this may have important implications for the emergence of infectious diseases. Moreover, overuse of antibiotics on crop fields results in drug-resistant plant bacteria, which may have a significant impact on our health.

Materials and methods

Mice and bacterial infection

All animal-related procedures were reviewed and approved by the Institutional Animal Care and Use Committee (IACUC) of the Korea Research Institute of Bioscience and Biotechnology (KRIBB), and were performed in accordance with institutional (National Institutes of Health, USA) guidelines for animal care. C57BL/6 mice were purchased from Jackson Laboratories. The experimental groups were all age- and sex-matched. Mice were injected intraperitoneally (i.p.) with bacteria (5.0×10^6 CFUs/g) at the age of 10 to 12 weeks. Bacterial strains were cultured in the growth medium and resuspensed at sterile PBS solution. *P. syringae* pv. *tomato* DC3000 and *P. syringae* pv. *tabaci* were grown for 24 h in King's B medium (King *et al.*, 1954). To generate GFP-expressing bacteria, pathovars of *P. syringae* were transformed with pDSK-GFPuv (Km^R).

TUNEL assay, tissue staining and blood analysis

Tissues were fixed in formalin and embedded in paraffin prior to sectioning (5 μm thick). Paraffin sections were then counterstained with H&E staining (haematoxylin and eosin staining). The TUNEL assay was performed using the DeadEnd Colorimetric TUNEL System (Promega), according to the manufacturer's instructions. Paraffin-embedded sections were deparaffinized for 5 min in xylene, rehydrated by immersion in a graded ethanol series, and fixed for 15 min in 4% paraformaldehyde in PBS. Tissue sections were permeabilized by incubation for 20 min at room temperature in 100 μl of proteinase K solution (20 g/ml). All steps were performed according to the manufacturer's instructions. Blood AST and ALT levels were analysed using an automated blood chemistry analyzer (Hitachi 7150).

Preparation of peritoneal macrophages and cell culture

Mouse peritoneal macrophages were harvested and cultured as described previously (Park *et al*., 2013; Yoon *et al*., 2015). RAW 264.7 murine macrophages were purchased from the American Type Culture Collection and grown in RPMI 1640 medium (ThermoFisher Scientific/Gibco) containing 10% fetal bovine serum (FBS; HyClone). 293T cells were grown in DMEM (HyClone) supplemented with 10% FBS. 3T3-L1 cells were grown in DMEM supplemented with 10% fetal calf serum and antibiotics. The absence/presence of Mycoplasma was determined by PCR. All cell lines were Mycoplasma-free.

Bacterial strains, plasmids and transformation

P. syringae pv. *tomato* (*Pto*) DC3000, the *P. syringae* pv. *tomato* (*Pto*) DC3000 Δ*hrpL* mutant, *P. syringae* pv. *tabaci* and *P. fluorescens* were cultured in King's B broth at 28 °C (Supporting Information Table S1). *E. coli* DH5α and *E. cloacae* were cultured in Lysogeny broth and nutrient broth, respectively, at 37 °C. The pDSK-GFPuv vector (green fluorescence) was introduced into bacteria by electroporation (Choi *et al*., 2006). The *P. fluorescens* type III effector strains are described in Supporting Information Table S1. The pBBRBB-DsRED (red fluorescence) and pBICEP-hopQ1-1 vectors were introduced into *E. cloacae* by electroporation (300 mM sucrose was replaced with 10% glycerol).

Cloning and transfection

The pEBG and pBICEP vectors (Sigma) were used to generate GST-LIMK1 and FLAG-HopQ1 in 293T cells. The pLVX-mCherry-N1 vector (Clontech) was used to generate mCherry-tagged HopQ1 in 3T3-L1 cells (Supporting Information Table S2). All cloning was performed using the In-Fusion HD Cloning Kit (Clontech), as recommended by the manufacturer. Cells were plated in 6-well plates at a density of 1.0×10^6 cells per well. After culture for 24 h at 37 °C to adjust to the transfection conditions, cells were incubated for 24 h at 37 °C with DNA-polymer complexes using the TransIT-X2 Dynamic Delivery System reagent (Mirus Bio).

Flow cytometry analysis of phagocytosis

Peritoneal macrophages and RAW 264.7 cells were plated in 12-well plates (density, 1.0×10^6 cells per well) and then infected with 2.0×10^7 CFUs of each GFP-

expressing bacterium. After the indicated times, the wells were washed three times with cold PBS to remove any remaining bacteria. Cells were then scraped from the wells and analysed immediately using a FACSCanto II flow cytometer (BD Biosciences). In total, 10 000 events per sample were collected and data were analysed using FlowJo software v10.1.

Immunostaining

Peritoneal macrophages (1.0×10^5 cells per well) were plated on round glass cover slips in 24-well plates and infected with bacteria (2.0×10^6 CFUs). After infection, cells were washed with cold PBS and fixed for 15 min at room temperature in 4% paraformaldehyde in PBS. Nuclei were stained for 5 min at room temperature with 4′,6-diamidino-2-phenylindole (DAPI; ThermoFisher Scientific), and the cells were washed again with cold PBS. Prior to staining with primary antibodies, cells were permeabilized for 10 min at room temperature in 0.2% Triton X-100 in PBS and then incubated overnight at 4 °C with antibodies specific for Rab5 (Cell Signalling Technology) or GST (Santa Cruz Biotechnology). Cells were then washed with PBS and incubated for 2 h at room temperature with Alexa Fluor 488-conjugated donkey-anti-rabbit IgG (Abcam). To stain F-actin, cells were incubated for 30 min at room temperature with Alexa Fluor 555-conjugated phalloidin (ThermoFisher Scientific). After bacterial infection, live cells were incubated for 30 min at room temperature with LysoTracker Red DND-99 (ThermoFisher Scientific). Images were obtained using an LSM510 confocal microscope (Carl Zeiss).

Western blotting, immunoprecipitation and GST pull-down assays

Western blot analyses of cell lysates were performed as described previously (Park *et al*., 2013; Yoon *et al*., 2015). Antibodies specific for p-JNK (4668), JNK (9258), pNF-κB p65 (3033), NF-κB p65 (4764), p-Erk1/2 (4370), Erk1/2 (9102), p-p38 (9215), p38 (9212), Eea1 (3288), Rab5 (3547), Rab7 (9367) and chronophin (4686) were purchased from Cell Signalling Technology. Antibodies specific for pleckstrin (sc-136042), Lamp1 (sc-19992) and β-actin (sc-47778) were purchased from Santa Cruz Biotechnology. The anti-Flag antibody was purchased from Sigma. For immunoprecipitation, cell lysates were incubated for 2 h at 4 °C with anti-DYKDDDDK (Flag)-tagged magnetic beads (Clontech Laboratories) on a rotating apparatus. The beads were then washed three times with cold lysis buffer, followed by an equal amount of 2× Laemmli sample buffer. To identify binding partners, antibodies specific for Limk1 (3842), p-Limk1 (3841), p-cofilin1 (3313), cofilin1 (5175), Ssh1 (13578) and Pak1 (2602) were purchased from Cell Signalling Technology. Antibodies specific for Cdc42 (sc-8401) and Rac1 (sc-217) were purchased from Santa Cruz Biotechnology. For the GST pull-down assay, cell lysates were incubated for 1 h at room temperature with glutathione MagBeads (GenScript), followed by washing three times in cold lysis buffer. An equal amount of 2× Laemmli sample buffer was then added to the beads. Antibodies bound to HopQ1 were detected using an anti-Flag antibody (Sigma).

ELISA

Cytokines (TNF-α, IL-1β and IL-6) secreted into the culture medium were measured using DuoSet antibody pairs (R&D Systems). Colour was developed with a 3,3′,5,5′-tetramethylbenzidine (TMB) substrate reagent set (BD Biosciences), and absorbance was measured at 450 nm in a microtiter plate reader (Emax; Molecular Devices).

Gentamicin protection assay

Macrophages were inoculated with each bacterium for 1 h, treated with gentamicin for 1 h and then washed with cold PBS to remove adherent bacteria from the cell surface. The cells were lysed for 15 min at room temperature in PBS containing 1.0% Triton X-100. The lysates were then plated on agar plates and incubated for 20 h at 37 °C, or at 30 °C in the case of plant bacteria.

Phagocytic cup formation

RAW 264.7 cells were seeded in Ibidi high 35 mm μ-dishes (Ibidi) (density, 1×10^5 cells/dish). After 24 h, cells were incubated with fresh culture medium and transferred to a live cell incubating chamber (Live Cell Instrument) at 37 °C under an atmosphere of 5% CO_2. The chamber was set on the stage of an inverted fluorescence microscope (IX81-ZDC; Olympus) fitted with a UPLSAPO 20× objective lens. Bacteria, either WT or Δ*hrpL*, were added to the culture dishes prior to live image analysis. Phagocytic cup formation by RAW 264.7 cells was monitored every 15 s over a 30 min period. Data analysis was performed using MetaMorph software, version 7.1 (Universal Imaging).

Statistical analysis

All data are expressed as the mean ± SD. Differences between averages were analysed using Student's *t* test. The significance of differences in survival was determined using the log-rank test.

Acknowledgements

This work was supported by grants from the KRIBB Research Initiative Program, Republic of Korea, the Woo Jang-Choon Project (PJ002015) of the Rural Development Administration and the National Research Foundation (NRF), which is funded by the Korean government (MSIP) (NRF-2015M3A9E6028953), South Korea.

Conflict of interest

The authors declare no competing financial interests.

Author contribution

S.-J.Y., Y.-J.P. and C.-M.R. designed and performed experiments and analysed data. S.H.L., S.-H.L. and S.C. provided technical assistance. S.-H.L. and J.-K.M. carried out the animal studies. Y.-J.P., C.-M.R. and I.P.C. supervised the project. S.-J.Y., Y.-J.P., J.-S.K. and C.-M.R. wrote the manuscript.

References

Alfano, J.R., and Collmer, A. (1997) The type III (Hrp) secretion pathway of plant pathogenic bacteria: trafficking harpins, Avr proteins, and death. *J Bacteriol* **179**: 5655–5662.

Ausubel, F.M. (2005) Are innate immune signaling pathways in plants and animals conserved? *Nat Immunol* **6**: 973–979.

van Baarlen, P., van Belkum, A., Summerbell, R.C., Crous, P.W., and Thomma, B.P. H.J. (2007) Molecular mechanisms of pathogenicity: how do pathogenic microorganisms develop cross-kingdom host jumps? *FEMS Microbiol Rev* **31**: 239–277.

Bierne, H., Gouin, E., Roux, P., Caroni, P., Yin, H.L., and Cossart, P. (2001) A role for cofilin and LIM kinase in listeria-induced phagocytosis. *J Cell Biol* **155**: 101–112.

Birkenfeld, J., Betz, H., and Roth, D. (2003) Identification of cofilin and LIM-domain-containing protein kinase 1 as novel interaction partners of 14-3-3zeta. *Biochem J* **369**: 45–54.

Blanchoin, L., Boujemaa-Paterski, R., Sykes, C., and Plastino, J. (2014) Actin dynamics, architecture, and mechanics in cell motility. *Physiol Rev* **94**: 235–263.

Bravo-Cordero, J.J., Magalhaes, M.A.O., Eddy, R.J., Hodgson, L., and Condeelis, J. (2013) Functions of cofilin in cell locomotion and invasion. *Nat Rev Mol Cell Biol* **14**: 405–415.

Choi, K.-H., Kumar, A., and Schweizer, H.P. (2006) A 10-min method for preparation of highly electrocompetent Pseudomonas aeruginosa cells: application for DNA fragment transfer between chromosomes and plasmid transformation. *J Microbiol Methods* **64**: 391–397.

Coburn, B., Sekirov, I., and Finlay, B.B. (2007) Type III secretion systems and disease. *Clin Microbiol Rev* **20**: 535–549.

Coppolino, M.G., Krause, M., Hagendorff, P., Monner, D.A., Trimble, W., Grinstein, S, *et al*. (2001) Evidence for a molecular complex consisting of Fyb/SLAP, SLP-76, Nck, VASP and WASP that links the actin cytoskeleton to Fcgamma receptor signalling during phagocytosis. *J Cell Sci* **114**: 4307–4318.

Cunnac, S., Lindeberg, M., and Collmer, A. (2009) Pseudomonas syringae type III secretion system effectors: repertoires in search of functions. *Curr Opin Microbiol* **12**: 53–60.

Day, B., Henty, J.L., Porter, K.J., and Staiger, C.J. (2011) The pathogen-actin connection: a platform for defense signaling in plants. *Annu Rev Phytopathol* **49**: 483–506.

Flannagan, R.S., Cosío, G., and Grinstein, S. (2009) Antimicrobial mechanisms of phagocytes and bacterial evasion strategies. *Nat Rev Microbiol* **7**: 355–366.

Frischknecht, F., Moreau, V., Röttger, S., Gonfloni, S., Reckmann, I., Superti-Furga, G., and Way, M. (1999) Actin-based motility of vaccinia virus mimics receptor tyrosine kinase signalling. *Nature* **401**: 926–929.

Galkin, V.E., Orlova, A., Kudryashov, D.S., Solodukhin, A., Reisler, E., Schroder, G.F., and Egelman, E.H. (2011) Remodeling of actin filaments by ADF/cofilin proteins. *Proc Natl Acad Sci USA* **108**: 20568–20572.

Garrity-Ryan, L., Kazmierczak, B., Kowal, R., Comolli, J., Hauser, A., and Engel, J.N. (2000) The arginine finger domain of ExoT contributes to actin cytoskeleton disruption and inhibition of internalization of Pseudomonas aeruginosa by epithelial cells and macrophages. *Infect Immun* **68**: 7100–7113.

Giska, F., Lichocka, M., Piechocki, M., Dadlez, M., Schmelzer, E., Hennig, J., and Krzymowska, M. (2013) Phosphorylation of HopQ1, a type III effector from pseudomonas syringae, creates a binding site for host 14-3-3 proteins. *Plant Physiol* **161**: 2049–2061.

Gordon, S. (2016) Phagocytosis: an Immunobiologic process. *Immunity* **44**: 463–475.

Gouin, E., Gantelet, H., Egile, C., Lasa, I., Ohayon, H., Villiers, V., *et al*. (1999) A comparative study of the actin-based motilities of the pathogenic bacteria *Listeria monocytogenes*, Shigella flexneri and rickettsia conorii. *J Cell Sci* **112**: 1697–1708.

Guo, M., Kim, P., Li, G., Elowsky, C.G., and Alfano, J.R. (2016) A bacterial effector co-opts Calmodulin to target the plant microtubule network. *Cell Host Microbe* **19**: 67–78.

Hybiske, K., and Stephens, R.S. (2008) Exit strategies of intracellular pathogens. *Nat Rev Microbiol* **6**: 99–110.

Kinchen, J.M., and Ravichandran, K.S. (2008) Phagosome maturation: going through the acid test. *Nat Rev Mol Cell Biol* **9**: 781–795.

King, E.O., Ward, M.K., and Raney, D.E. (1954) Two simple media for the demonstration of pyocyanin and fluorescin. *J Lab Clin Med* **44**: 301–307.

Kirzinger, M.W.B., Nadarasah, G., and Stavrinides, J. (2011) Insights into cross-kingdom plant pathogenic bacteria. *Genes* **2**: 980–997.

Krzymińska, S., Mokracka, J., Koczura, R., and Kaznowski, A. (2009) Cytotoxic activity Of*enterobacter cloacae*human isolates. *FEMS Immunol Med Microbiol* **56**: 248–252.

Laroux, F.S., Romero, X., Wetzler, L., Engel, P., and Terhorst, C. (2005) Cutting edge: MyD88 controls

phagocyte NADPH oxidase function and killing of gram-negative bacteria. *J Immunol* **175**: 5596–5600.
Li, J., and Staiger, C.J. (2018) Understanding cytoskeletal dynamics during the plant immune response. *Annu Rev Phytopathol* **56**: 513–533.
Li, W., Chiang, Y.-H., and Coaker, G. (2013a) The HopQ1 Effector's nucleoside hydrolase-like domain is required for bacterial virulence in Arabidopsis and tomato, but not host recognition in tobacco. *PLoS One* **8**: e59684.
Li, W., Yadeta, K.A., Elmore, J.M., and Coaker, G. (2013b) The *Pseudomonas syringae* effector HopQ1 promotes bacterial virulence and interacts with tomato 14-3-3 proteins in a phosphorylation-dependent manner. *Plant Physiol* **161**: 2062–2074.
Medzhitov, R., and Janeway, C. (2000) Innate immunity. *New Engl J Med* **343**: 338–344.
Mizuno, K. (2013) Signaling mechanisms and functional roles of cofilin phosphorylation and dephosphorylation. *Cell Signal* **25**: 457–469.
Mostowy, S., and Shenoy, A.R. (2015) The cytoskeleton in cell-autonomous immunity: structural determinants of host defence. *Nat Rev Immunol* **15**: 559–573.
Nurnberger, T., Brunner, F., Kemmerling, B., and Piater, L. (2004) Innate immunity in plants and animals: striking similarities and obvious differences. *Immunol Rev* **198**: 249–266.
Okano, I., Hiraoka, J., Otera, H., Nunoue, K., Ohashi, K., Iwashita, S., *et al*. (1995) Identification and characterization of a novel family of serine/threonine kinases containing two N-terminal LIM motifs. *J Biol Chem* **270**: 31321–31330.
Pan, X., Yang, Y., and Zhang, J.-R. (2014) Molecular basis of host specificity in human pathogenic bacteria. *Emerg Microbes Infect* **3**: e23–e23.
Park, Y.-J., Yoon, S.-J., Suh, H.-W., Kim, D.O., Park, J.-R., Jung, H., *et al*. (2013) TXNIP deficiency exacerbates Endotoxic shock via the induction of excessive nitric oxide synthesis. *PLoS Pathog* **9**: e1003646.
Porter, K., and Day, B. (2015) From filaments to function: the role of the plant actin cytoskeleton in pathogen perception, signaling and immunity. *J Integr Plant Biol* **58**: 299–311.
Prasadarao, N.V., Blom, A.M., Villoutreix, B.O., and Linsangan, L.C. (2002) A novel interaction of outer membrane protein a with C4b binding protein mediates serum resistance of *Escherichia coli* K1. *J Immunol* **169**: 6352–6360.
Rooijakkers, S.H.M., Ruyken, M., Roos, A., Daha, M.R., Presanis, J.S., Sim, R.B., *et al*. (2005) Immune evasion by a staphylococcal complement inhibitor that acts on C3 convertases. *Nat Immunol* **6**: 920–927.
Sarantis, H., and Grinstein, S. (2012) Subversion of phagocytosis for pathogen survival. *Cell Host Microbe* **12**: 419–431.
Selosse, M.-A., Bessis, A., and Pozo, M.J. (2014) Microbial priming of plant and animal immunity: symbionts as developmental signals. *Trends Microbiol* **22**: 607–613.
Settembre, C., Fraldi, A., Medina, D.L., and Ballabio, A. (2013) Signals from the lysosome: a control Centre for cellular clearance and energy metabolism. *Nat Rev Mol Cell Biol* **14**: 283–296.
Shimono, M., Lu, Y.-J., Porter, K., Kvitko, B.H., Henty-Ridilla, J., Creason, A, *et al*. (2016) The pseudomonas syringae type III effector HopG1 induces actin remodeling to promote symptom development and susceptibility during infection. *Plant Physiol* **171**: 2239–2255.
Sreedharan, A., Penaloza-Vazquez, A., Kunkel, B.N., and Bender, C.L. (2006) CorR regulates multiple components of virulence in pseudomonas syringae pv.Tomato DC3000. *Mol Plant Microbe Interact* **19**: 768–779.
Stevens, J.M., Galyov, E.E., and Stevens, M.P. (2006) Actin-dependent movement of bacterial pathogens. *Nat Rev Microbiol* **4**: 91–101.
Swanson, J.A. (2008) Shaping cups into phagosomes and macropinosomes. *Nat Rev Mol Cell Biol* **9**: 639–649.
Underhill, D.M., and Goodridge, H.S. (2012) Information processing during phagocytosis. *Nat Rev Immunol* **12**: 492–502.
Wang, Y., Li, J., Hou, S., Wang, X., Li, Y., Ren, D, *et al*. (2010) A pseudomonas syringae ADP-Ribosyltransferase inhibits Arabidopsis mitogen-activated protein kinase kinases. *Plant Cell* **22**: 2033–2044.
Whittaker, J.H., Robertson, A.P., Kimber, M.J., Day, T.A., and Carlson, S.A. (2016) Intestinal Enterobacteriaceae that protect nematodes from the effects of Benzimidazoles. *J Bacteriol Parasitol* **07**: 5.
Xin, X.-F., and He, S.Y. (2013) Pseudomonas syringae pv. Tomato DC3000: a model pathogen for probing disease susceptibility and hormone signaling in plants. *Annu Rev Phytopathol* **51**: 473–498.
Yoon, S.-J., Park, J.-Y., Choi, S., Lee, J.-B., Jung, H., Kim, T.-D., *et al*. (2015) Ginsenoside Rg3 regulates S-nitrosylation of the NLRP3 inflammasome via suppression of iNOS. *Biochem Biophys Res Commun* **463**: 1184–1189.
Zhang, J., Shao, F., Li, Y., Cui, H., Chen, L., Li, H., *et al*. (2007) A pseudomonas syringae effector inactivates MAPKs to suppress PAMP-induced immunity in plants. *Cell Host Microbe* **1**: 175–185.

Supporting Information

Additional Supporting Information may be found in the online version of this article at the publisher's web-site:

Appendix S1: Supplemental Materials